Draft version December 19, 2018
Typeset using LaTeX **twocolumn** style in AASTeX62

A HOT SATURN ORBITING AN OSCILLATING SUBGIANT DISCOVERED BY TESS

Daniel Huber,[1] William J. Chaplin,[2,3] Ashley Chontos,[1,4] Hans Kjeldsen,[3] Jørgen Christensen-Dalsgaard,[3] Timothy R. Bedding,[5,3] Warrick Ball,[2] Rafael Brahm,[6,7] Nestor Espinoza,[8] Thomas Henning,[8] Andrés Jordán,[6,7] Frank Grundahl,[3] Mads Fredslund Andersen,[3] Emil Knudstrup,[3] Simon Albrecht,[3] Ian Crossfield,[9] Benjamin Fulton,[10] Andrew W. Howard,[10] Howard T. Isaacson,[11] Lauren M. Weiss,[1] Rasmus Handberg,[3] Mikkel Lund,[3] Aldo M. Serenelli,[12,13] David W. Latham,[14] Allyson Bierlya,[14] Samuel N. Quinn,[14] Eric Gaidos,[15] Teruyuki Hirano,[16,1] George R. Ricker,[9] Roland K. Vanderspek,[9] Sara Seager,[9,17] Jon M. Jenkins,[18] Joshua N. Winn,[19] H. M. Antia,[20] Sarbani Basu,[21] Keaton Bell,[22,3] Othman Benomar,[23] Alfio Bonanno,[24] Derek L. Buzasi,[25] Tiago L. Campante,[26,27] Z. Çelik Orhan,[28] Enrico Corsaro,[24] Margarida S. Cunha,[26,27] Guy R. Davies,[2,3] Sebastien Deheuvels,[29,30] Samuel K. Grunblatt,[1] Maria Pia Di Mauro,[31] Rafael A. García,[32] Patrick Gaulme,[33,3] Léo Girardi,[34] Joyce Guzik,[35] Marc Hon,[36] Chen Jiang,[26,27] Thomas Kallinger,[37] Steven D. Kawaler,[38] James Kuszlewicz,[22,3] Yveline Lebreton,[39,40] Tanda Li,[5,3] Miles Lucas,[38] Mia Lundkvist,[3] Savita Mathur,[41] Anwesh Mazumdar,[42] Travis S. Metcalfe,[43] Andrea Miglio,[2,3] Mário J. P. F. G. Monteiro,[26,27] Benoit Mosser,[44] Benard Nsamba,[26,27] Joel Jia Mian Ong,[21] S. Örtel,[28] Felipe Pereira,[26,27] Pritesh Ranadive,[42] Clara Régulo,[41] Thaíse S. Rodrigues,[34,45] Jakob Lysgaard Rorsted,[3] Ian W. Roxburgh,[46] Victor Silva Aguirre,[3] Barry Smalley,[47] Mathew Schofield,[2,3] Keivan G. Stassun,[48,49] Dennis Stello,[36,5,3] Amalie Stokholm,[3] Jamie Tayar,[1] Timothy R. White,[3] Kuldeep Verma,[3] Mathieu Vrard,[26] M. Yildiz,[28] Bryson Cale,[50] Roberto Carlino,[51] Jason A. Dittmann,[14] Gabor Furesz,[9] Jonathan Gagne,[52] Peter Gao,[11] Frank Giddens,[53] Natasha Latouf,[50] Danny Lebrun,[50] Al Levine,[9] Andrew Mann,[54] William Matzko,[50] Peter Plavchan,[50] Masoud Mansouri-Samani,[51] Sean McCauliff,[55] Scott Mcdermott,[56] Aylin Garcia Soto,[57] Martin Paegert,[14] Angelle Tanner,[58] Johanna Teske,[59,60] and Sharon Xuesong Wang[59]

[1] *Institute for Astronomy, University of Hawai'i, 2680 Woodlawn Drive, Honolulu, HI 96822, USA*

[2] *School of Physics and Astronomy, University of Birmingham, Birmingham B15 2TT, UK*

[3] *Stellar Astrophysics Centre (SAC), Department of Physics and Astronomy, Aarhus University, Ny Munkegade 120, DK-8000 Aarhus C, Denmark*

[4] *NSF Graduate Research Fellow*

[5] *Sydney Institute for Astronomy (SIfA), School of Physics, University of Sydney, NSW 2006, Australia*

[6] *Instituto de Astrofísica, Facultad de Física, Pontificia Universidad Católica de Chile, Av. Vicuña Mackenna 4860, 7820436 Macul, Santiago, Chile*

[7] *Millennium Institute of Astrophysics, 7820436 Santiago, Chile*

[8] *Max-Planck-Institut fur Astronomie, Königstuhl 17, D-69117 Heidelberg, Germany*

[9] *Department of Physics, and Kavli Institute for Astrophysics and Space Research, Massachusetts Institute of Technology, Cambridge, MA 02139, USA*

[10] *California Institute of Technology, Pasadena, CA 91125, USA*

[11] *Department of Astronomy, UC Berkeley, Berkeley, CA 94720, USA*

[12] *Institut dEstudis Espacials de Catalunya (IEEC), C/Gran Capita, 2-4, E-08034, Barcelona, Spain*

[13] *Institute of Space Sciences (ICE, CSIC) Campus UAB, Carrer de Can Magrans, s/n, E-08193, Barcelona, Spain*

[14] *Harvard-Smithsonian Center for Astrophysics, Cambridge, Massachusetts 02138, USA*

[15] *Department of Geology & Geophysics, University of Hawaii at Manoa, Honolulu, Hawaii 96822, USA*

[16] *Department of Earth and Planetary Sciences, Tokyo Institute of Technology, 2-12-1 Ookayama, Meguro-ku, Tokyo 152-8551, Japan*

[17] *Earth and Planetary Sciences, MIT, 77 Massachusetts Avenue, Cambridge, MA 02139, USA*

[18] *NASA Ames Research Center, Moffett Field, CA, 94035*

[19] *Princeton University, Princeton, NJ 08540, USA*

[20] *Tata Institute of Fundamental Research, Mumbai, India*

[21] *Department of Astronomy, Yale University, P.O. Box 208101, New Haven, CT 06520-8101, USA*

[22] *Max-Planck-Institut fur Sonnensystemforschung, Justus-von-Liebig-Weg 3, 37077 Gottingen, Germany*

[23] *Center for Space Science, New York University Abu Dhabi, UAE*

[24] *INAF - Osservatorio Astrofisico di Catania, via S. Sofia 78, 95123, Catania, Italy*

huberd@hawaii.edu

w.j.chaplin@bham.ac.uk

[25] Dept. of Chemistry & Physics, Florida Gulf Coast University, 10501 FGCU Blvd. S., Fort Myers, FL 33965 USA
[26] Instituto de Astrofisica e Ciencias do Escaco, Universidade do Porto, Rua das Estrelas, PT4150-762 Porto, Portugal
[27] Departamento de Fisica e Astronomia, Faculdade de Ciencias da Universidade do Porto, Rua do Campo Alegre, s/n, PT4169-007 Porto, Portugal
[28] Department of Astronomy and Space Sciences, Science Faculty, Ege University, 35100, Bornova, İzmir, Turkey
[29] Université de Toulouse; UPS-OMP; IRAP; Toulouse, France
[30] CNRS; IRAP; 14, avenue Edouard Belin, F-31400 Toulouse, France
[31] INAF-IAPS, Istituto di Astrofisica e Planetologia Spaziali, Via del Fosso del Cavaliere 100, I-00133 Roma, Italy
[32] Laboratoire AIM, CEA/DSM-CNRS, Université Paris 7 Diderot, IRFU/SAp, Centre de Saclay, 91191, Gif-sur-Yvette, France
[33] 1Max-Planck-Institut fur Sonnensystemforschung, Justus-von-Liebig-Weg 3, 37077 Gottingen, Germany
[34] Osservatorio Astronomico di Padova INAF, Vicolo dellOsservatorio 5, I-35122 Padova, Italy
[35] Los Alamos National Laboratory, XTD-NTA, MS T-082, Los Alamos, NM 87545 USA
[36] School of Physics, The University of New South Wales, Sydney NSW 2052, Australia
[37] Institute of Astronomy, University of Vienna, 1180 Vienna, Austria
[38] Department of Physics and Astronomy, Iowa State University, Ames, IA 50011 USA
[39] Observatoire de Paris, GEPI, CNRS UMR 8111, F-92195 Meudon, France 2
[40] Institut de Physique de Rennes, Universite de Rennes 1, CNRS UMR 6251, F-35042 Rennes, France
[41] Instituto de Astrofisica de Canarias, 38205 La Laguna, Tenerife, Spain
[42] Homi Bhabha Centre for Science Education, TIFR, V. N. Purav Marg, Mankhurd, Mumbai 400088, India
[43] Space Science Institute, 4750 Walnut Street, Suite 205, Boulder CO 80301, USA
[44] LESIA, CNRS, Université Pierre et Marie Curie, Université Denis, Diderot, Observatoire de Paris, 92195 Meudon cedex, France
[45] Dipartimento di Fisica e Astronomia, Università di Padova, Vicolo dellOsservatorio 2, I-35122 Padova, Italy
[46] Astronomy Unit, Queen Mary University of London, Mile End Road, London, E1 4NS, UK
[47] Astrophysics Group, Lennard-Jones Laboratories, Keele University, Staffordshire ST5 5BG, United Kingdom
[48] Vanderbilt University, Department of Physics & Astronomy, 6301 Stevenson Center Ln., Nashville, TN 37235, USA
[49] Vanderbilt Initiative in Data-intensive Astrophysics (VIDA), 6301 Stevenson Center Lane, Nashville, TN 37235, USA
[50] Department of Physics and Astronomy, George Mason University 4400 University Ave, Fairfax, VA 22030
[51] SGT Inc/NASA Ames Research Center, Moffett Field, CA, 94035
[52] Carnegie Institution of Washington DTM, 5241 Broad Branch Road NW, Washington, DC 20015, USA
[53] Missouri State University
[54] Department of Physics and Astronomy, University of North Carolina at Chapel Hill, Chapel Hill, NC 27599-3255, USA
[55] Wyle Labs/NASA Ames Research Center, Moffett Field, CA, 94035
[56] Proto Logic?
[57] Wesleyan
[58] Mississippi State University, Department of Physics & Astronomy, Hilbun Hall, Starkville, MS, 39762, USA
[59] Department of Terrestrial Magnetism, Carnegie Institution for Science, 5241 Broad Branch Road, NW, Washington, DC 20015
[60] Observatories of the Carnegie Institution for Science, 813 Santa Barbara Street, Pasadena, CA 91101

ABSTRACT

We present the discovery of TOI-197.01, the first transiting planet orbiting an oscillating host star identified by the *Transiting Exoplanet Survey Satellite* (*TESS*). TOI-197 (HIP 116158) is a bright ($V = 8.2$ mag) subgiant which oscillates with an average frequency of $\approx 430\,\mu$Hz and displays a clear signature of mixed modes. The oscillation amplitude is consistent with the Kepler sample, indicating that the redder bandpass of *TESS* only has a small effect on the detectability of oscillations. Asteroseismic modeling yields a robust characterization of the host star radius ($R_\star = 2.936 \pm 0.061 R_\odot$), mass ($M_\star = 1.198 \pm 0.081 M_\odot$) and age ($5.04 \pm 1.26$ Gyr), demonstrating that it has just started its ascent on the red giant branch. Combining the asteroseismology with transit modeling and radial-velocity observations show that the planet is a hot Saturn ($P = 14.3$ d, $F = 344 \pm 27 F_\oplus$, $R_\mathrm{p} = 0.841 \pm 0.031\,R_\mathrm{J}$) with moderate density ($M_\mathrm{p} = 0.191 \pm 0.017\,M_\mathrm{J}$, $\rho_\mathrm{p} = 0.424 \pm 0.060\,\mathrm{g\,cm^{-3}}$). TOI-197.01 deviates from the host-star metallicity – planet mass correlation found in sub-Saturns and may indicate that planets in the transition region between sub-Saturns and Jupiters follow a relatively narrow range of densities. With a density measured to $\approx 15\%$ TOI-197.01 is one the best characterized Saturn-sized planets to date, joining a small sample of transiting planets around evolved stars and demonstrating the strong potential of asteroseismology to characterize exoplanets and their host stars with *TESS*.

Keywords: planets and satellites: individual (TOI-197) — stars: fundamental parameters — techniques: asteroseismology, photometry, spectroscopy — TESS — planetary systems

1. INTRODUCTION

Asteroseismology is one of the major success stories of the space photometry revolution initiated by CoRoT and *Kepler*. The detection of oscillations in hundreds of solar-type stars has led to breakthroughs such as the discovery of rapidly rotating cores in subgiants and the systematic measurement of stellar masses, radii and ages (see Chaplin & Miglio 2013, for a review). Asteroseismology has also become the "gold-standard" for calibrating more indirect methods to determine fundamental stellar parameters, including surface gravities ($\log g$) from spectroscopy (Petigura et al. 2017a), stellar granulation (Bastien et al. 2013), and ages from rotation periods (gyrochronology, e.g. van Saders et al. 2016).

A remarkable synergy that emerged from space-based photometry is the systematic characterization of exoplanet host stars using asteroseismology. Following first asteroseismic studies of exoplanet host stars using radial-velocities (Bouchy et al. 2005; Bazot et al. 2005), the Hubble Space Telescope (Gilliland et al. 2011) and CoRoT (Ballot et al. 2011; Lebreton & Goupil 2014), *Kepler* enabled the systematic characterization of exoplanets with over 100 detections to date (Huber et al. 2013a; Lundkvist et al. 2016). In addition to the precise characterization of exoplanet radii and masses (Ballard et al. 2014), the synergy also enabled systematic constraints on stellar spin-orbit alignments (Chaplin et al. 2014; Benomar et al. 2014; Campante et al. 2016; Lund et al. 2016) and statistical inferences on orbital eccentricities through constraints on the mean stellar density (Sliski & Kipping 2014; Van Eylen & Albrecht 2015; Van Eylen et al. 2018).

The recently launched NASA *TESS* Mission (Ricker et al. 2014) is poised to continue the synergy between asteroseismology and exoplanet science. Using dedicated 2-minute cadence sampling *TESS* is expected to detect oscillations in thousands of main-sequence and subgiant stars (Schofield et al. 2018), and simulations predict that at least 100 of these will host transiting or non-transiting exoplanets (Campante et al. 2016). *TESS* host stars are on average significantly brighter than typical Kepler hosts, facilitating ground-based measurements of planet masses with precisely characterized exoplanet hosts from asteroseismology. Here, we present the characterization of the TOI-197 (HIP 116158) system, the first discovery of a transiting exoplanet around an oscillating host star by *TESS*.

2. OBSERVATIONS

2.1. *TESS Photometry*

TESS observed TOI-197 in 2-minute cadence during Sector 2 of Cycle 1 for a total of 27 days. We used the target pixel files released on MAST[1] as part of the TESS alerts on November 11 2018. We produced a light curve using the photometry pipeline[2] (Handberg et al., in prep.) maintained by the TESS Asteroseismic Science Operations Center[3] (TASOC, Lund et al. 2017), which is an extended version of software originally developed to generate light curves for data collected by the K2 Mission (Lund et al. 2015).

Figure 1a shows the raw light curve obtained from the TASOC pipeline. The coverage is nearly continuous (duty cycle $\approx 93\,\%$), with a ≈ 2 day gap separating the two orbits in the observing sector. Two $\approx 0.1\,\%$ brightness dips, which triggered the identification of TOI-197.01 as a planet candidate, are evident near the beginning of each orbit. The structure with a period of ≈ 2.5 d corresponds to instrumental variations due to angular momentum dumps.

To prepare the raw light curve for an asteroseismic analysis, the current TASOC pipeline implements a series of corrections as described by Handberg & Lund (2014), which includes a removal of instrumental signals and of the transit events using a combination of filters utilising the estimated planetary period. Future TASOC-prepared light curves from full TESS data releases will include information from the ensemble of stars to remove common instrumental systematics (Lund et al, in prep.). The corrected light curve is shown in Figure 1b. Figure 1c shows a power spectrum of this light curve, revealing the clear presence of a granulation background and power excess near $\approx 430\,\mu$Hz, characteristic of solar-like oscillations of an evolved subgiant star near the base of the red-giant branch.

2.2. *High-Resolution Spectroscopy*

We initiated high-resolution spectroscopic follow-up of TOI-197 using several facilities within the TESS Follow-up Observation Program (TFOP), including HIRES (Vogt et al. 1994) on the 10-m telescope at Keck Observatory (Maunakea, Hawaii), SONG on the Hertzsprung

[1] https://archive.stsci.edu/prepds/tess-data-alerts/index.html
[2] https://tasoc.dk/code/
[3] https://tasoc.dk

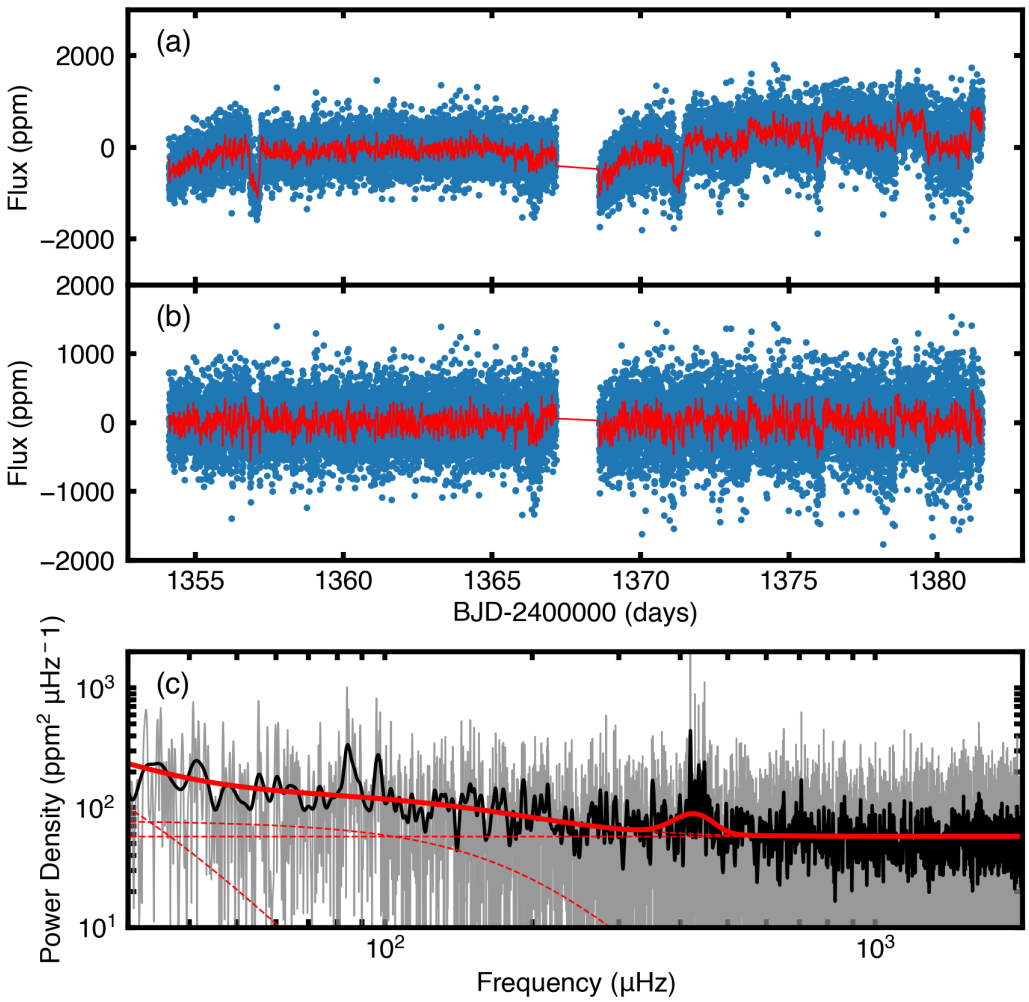

Figure 1. Panel (a): Raw TESS 2-minute cadence light curve of TOI-197 produced using aperture photometry by the TESS Asteroseismic Science Operations Center (TASOC). The red line shows the light curve smoothed with a 10-minute boxcar filter. Panel (b): Light curve after applying corrections by the TASOC pipeline. Panel (c): Power spectrum of the light curve in panel (b), showing a granulation background and a clear power excess due to solar-like oscillations near $\sim 430\mu$Hz. The solid red line shows the combined background fit, with individual components shown as dashed red lines.

Telescope at Teide Observatory (Tenerife) (Grundahl et al. 2017), FEROS on the MPG/ESO-2.2m Telescope at La Silla (Kaufer et al. 1999), Coralie on the 1.2-metre Leonhard Euler Telescope at La Silla (ref), TRES (Fürész 2008) on the 1.5-m Tillinghast reflector at the F. L. Whipple Observatory (Mt. Hopkins, Arizona), and iSHELL on the NASA IRTF Telescope on Maunakea (ref) [**observers: please correct/suggest additional references here**]. All spectra used in this paper have been obtained between Nov 11 – Dec xx 2018 and have a minimum spectral resolution of $R \approx 44000$. Most instruments have been previously used to obtain precise radial velocities to confirm exoplanets.

In addition to radial velocities, we used a Keck/HIRES spectrum to obtain atmospheric parameters using Spectmatch (Petigura et al. 2017a), which has been extensively applied for the classification of Kepler exoplanet host stars (Johnson et al. 2017; Fulton et al. 2017). The resulting parameters were $T_{\rm eff} = 5080 \pm 70$ K, $\log g = 3.60 \pm 0.08$ dex, [Fe/H] $= -0.08 \pm 0.08$ dex and $v \sin i = 2.8 \pm 1.6$km/s, consistent with an evolved star as identified from the power spectrum in Figure 1c. To account for systematic differences between spectroscopic methods (Torres et al. 2012) we added 59 K in $T_{\rm eff}$ and 0.062 dex in [Fe/H] in quadrature to the formal uncertainties, yielding final values of $T_{\rm eff} = 5080 \pm 90$ K and [Fe/H] $= -0.08 \pm 0.08$ dex (Table 2).

2.3. *Broadband Photometry & Gaia Parallax*

We fitted the spectral energy distribution (SED) of TOI-197 using broadband photometry following the method described by Stassun & Torres (2016). We used NUV photometry from *GALEX*, $B_T V_T$ from *Tycho-2* (Høg et al. 2000), $BVgri$ from APASS, JHK_S from *2MASS* (Skrutskie et al. 2006), W1–W4 from *WISE* (Wright et al. 2010), and the G magnitude from *Gaia* (Evans et al. 2018). The data were fit using Kurucz atmosphere models, with $T_{\rm eff}$, [Fe/H] and extinction (A_V) as free parameters. We restricted A_V to the maximum line-of-sight value from the dust maps of Schlegel et al. (1998). The resulting fit yielded $T_{\rm eff} = 5090 \pm 85$ K, [Fe/H] $= -0.3 \pm 0.3$ dex, and $A_V = 0.09 \pm 0.02$ mag with reduced χ^2 of 1.9, in good agreement with spectroscopy. Integrating the (unreddened) model SED gives the bolometric flux at Earth of $F_{\rm bol} = 1.88 \pm 0.04 \times 10^{-8}$ erg s cm^{-2}. An independent SED fit using 2MASS, APASS9, USNO-B1 and WISE photometry and Kurucz models yielded excellent agreement, with $F_{\rm bol} = 1.83 \pm 0.09 \times 10^{-8}$ erg s cm^{-2} and $T_{\rm eff} = 5150 \pm 130$ K.

Combining the bolometric flux with the Gaia DR2 distance allows us to derive a near-model independent luminosity, a valuable constraint for asteroseismic modeling (see Section 3.3). Using a Gaia parallax of 10.5180 ± 0.0795 mas (adjusted by $+0.08$ mas to account for the zeropoint offset for nearby stars reported by Stassun & Torres (2018)) with the two methods described above yielded $L = 5.13 \pm 0.13 L_\odot$ and $L = 5.30 \pm 0.14 L_\odot$, respectively. We additionally derived a luminosity using `isoclassify` (Huber et al. 2017), adopting 2MASS K-band photometry, bolometric corrections from MIST isochrones (Choi et al. 2016) and the composite reddening map `mwdust` (Bovy et al. 2016), yielding $L = 5.03 \pm 0.13 L_\odot$. Our final adopted Gaia luminosity was the mean of these methods with scatter added in quadrature, yielding $L = 5.15 \pm 0.17 L_\odot$.

2.4. *Adaptive Optics Imaging*

TOI-197 was observed with the NIRC2 camera and Altair adaptive optics system on Keck-2 (Wizinowich et al. 2000) on UT 25 November 2018. Conditions were cloud-free but seeing was poor (0.8-2"). AO used the science target as the natural guide star, and images were obtained through a combination of a K-continuum plus $KP50_{1.5}$ filter using the narrow camera (10 mas pixel scale). Eight images (four each at two dither positions), each consisting of 50 co-adds of 0.2 sec each were obtained, with correlated double sampling mode and four reads. Frames were co-added and an average dark image obtained constructed from a set of darks with the identical integration time and sampling mode was subtracted. Flat fielding was performed using a dome flat obtained in the K' filter. "Hot" pixels were identified in the dark image and corrected by median filtering with a 5×5 box centered on each offending pixel in the science image. Only a single star appears in the images: numerical experiments in which "clones" of the stellar image reduced by a specified contrast ratio were added to the original image were performed. These show that we would have been able to detect companions as faint as $\Delta K = 5.8$ magnitudes as close as 0.4" to TOI-197, or 3.8 magnitudes as close as 0.2", or 1.8 magnitudes to 0.1". Thus, we can exclude any significant dilution (both for oscillation amplitudes and the depth of transit events) for TOI-197.

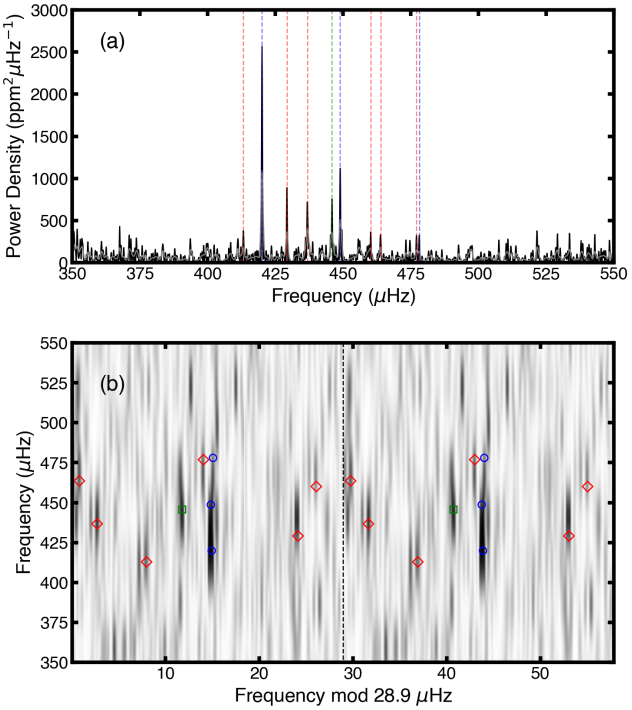

Figure 2. Panel (a): Power spectrum of TOI-197 centered on the frequency region showing oscillations. The grey line is a smoothed version with a Gaussian of width $\approx 0.3\,\mu$Hz. Panel (b): Greyscale échelle diagram of the background-corrected and smoothed power spectrum in panel (a). Identified individual frequencies are marked with blue circles ($l = 0$), green squares ($l = 2$) and red diamonds ($l = 1$).

3. ASTEROSEISMOLOGY

3.1. *Global Oscillation Parameters*

To extract oscillation parameters characterizing the average properties of the power spectrum we used several automated analysis methods (e.g Huber et al. 2009; Mathur et al. 2010; Mosser et al. 2012a; Stello et al. 2017;

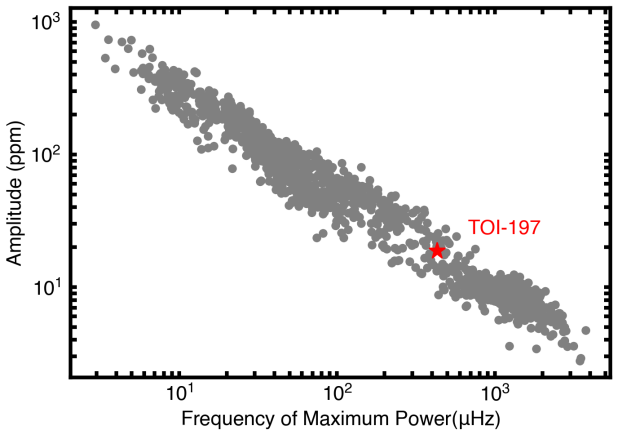

Figure 3. Amplitude per radial mode versus frequency of maximum power for a sample of ≈1500 stars spanning from the main-sequence to the red giant branch observed by Kepler (Huber et al. 2011). The red star shows the measured position of TOI-197.

Campante 2018; Bell et al. 2019) [**co-authors: please send preferred citations**], many of which have been extensively tested on *Kepler* data (e.g. Hekker et al. 2011; Verner et al. 2011). In summary, the power contribution due to granulation noise and stellar activity was typically modeled by a combination of power laws and a flat contribution due to shot noise, and then corrected by dividing the power spectrum by the background model. The individual contributions and final background model using the method by Huber et al. (2009) are shown as dashed and solid red lines in Figure 1c, and a close-up of the power excess is shown in Figure 2a.

Next, the frequency of maximum power ($\nu_{\rm max}$) was measured either by heavily smoothing the power spectrum or by fitting a Gaussian function to the power excess. Our analysis yielded $\nu_{\rm max} = 430 \pm 18\,\mu$Hz, with uncertainties calculated from the scatter over all methods. Finally, the mean oscillation amplitude per radial mode was determined by taking the peak of the smoothed, background corrected oscillation envelope and correcting for the contribution of non-radial modes (Kjeldsen et al. 2008), yielding $A = 18.7 \pm 3.5$ ppm. We caution that the $\nu_{\rm max}$ and amplitude estimates could be significantly biased by realization noise since the modes are not well resolved, as demonstrated by the non-Gaussian appearance of the power spectrum and the strong single peak near $\approx 420\,\mu$Hz.

Global seismic parameters such as $\nu_{\rm max}$ and amplitude follow well-known scaling relations (Huber et al. 2011; Mosser et al. 2012b; Corsaro et al. 2013), and thus allow us to test whether the detected oscillations are consistent with expectations. Figure 3 compares our measured $\nu_{\rm max}$ and amplitude with results for ≈1500 stars observed by *Kepler* (Huber et al. 2011). We observe excellent agreement, confirming that the detected signal is consistent with solar-like oscillations. We note that the oscillations in the TESS bandpass are expected to be $\approx 20\,\%$ smaller than in the Kepler bandpass, which is well within the spread of amplitudes at a given $\nu_{\rm max}$ observed in the *Kepler* sample. The result confirms that the redder bandpass of *TESS* only has a small effect on the oscillation amplitude, and validates the expected asteroseismic yield of thousands of detections of solar-like oscillators with TESS (Schofield et al. 2018).

3.2. *Individual Mode Frequencies*

The power spectrum in Figure 2a shows clear individual mode frequencies. Given that *TESS* instrument artifacts are not yet well understood, we restricted our analysis to the frequency range between 400-500μHz where we observe peaks well above the noise level.

To extract these individual mode frequencies, we used independent methods ranging from traditional iterative sine-wave fitting, i.e., pre-whitening (e.g. Kjeldsen et al. 2005; Bedding et al. 2007), to fitting of Lorentzian mode profiles (e.g., see (e.g. Appourchaux et al. 2012; Corsaro & De Ridder 2014; Davies & Miglio 2016; Kallinger et al. 2018) [**co-authors: please send preferred citations**]. We required at least two independent methods to return the same frequency within uncertainties and that the posterior probability of each peak being a mode was $\geq 90\,\%$ (Basu & Chaplin 2017). For the final list of frequencies we adopted values from one fitter (HK), with uncertainties derived from realistic Monte Carlo simulations of the data. A comparison of the frequencies returned by different fitters showed very good agreement, at a level smaller than the uncertainties for all the reported modes.

The final list of extracted frequencies is shown in Table 1. To measure the large frequency separation $\Delta\nu$, we performed a linear fit to all identified radial modes, yielding $\Delta\nu = 28.94 \pm 0.15\mu$Hz. Figure 2b shows a greyscale échelle diagram using this $\Delta\nu$ measurement, including the extracted mode frequencies. The $l = 1$ modes are strongly affected by mode bumping, as expected for the mixed mode coupling factors for evolved subgiants in this evolutionary stage. The offset of the $l = 0$ ridge ϵ is ≈ 0.5, consistent with the expected value from Kepler measurements for a star with similar $\Delta\nu$ and $T_{\rm eff}$ (White et al. 2011).

3.3. *Frequency Modeling*

Table 1. Extracted oscillation frequencies and mode identifications for TOI-197.

$f(\mu\text{Hz})$	$\sigma_f(\mu\text{Hz})$	l
413.12	0.29	1
420.06	0.11	0
429.26	0.14	1
436.77	0.24	1
445.85	0.21	2
448.89	0.21	0
460.16	0.33	1
463.81	0.43	1
477.08	0.31	1
478.07	0.35	0

Note: The large frequency separation derived from radial modes is $\Delta\nu = 28.94 \pm 0.15\mu$Hz.

We used a number of different codes and methods to model the observed oscillation frequencies, including MESA+Gyre (JJMG,TL,WB, Paxton et al. 2011, 2013, 2015; Choi et al. 2016; Creevey et al. 2017; Townsend & Teitler 2013), GARSTEC+BeSSP (AS, Serenelli et al. 2013, 2017), YREC (SB,JT, Demarque et al. 2008; Tayar & Pinsonneault 2018), Cesam2K (YL, Morel & Lebreton 2008; Scuflaire et al. 2008; Lebreton & Goupil 2014), Iben [JG, ref needed], GARSTEC+BASTA (AS,VSA, Silva Aguirre et al. 2015) and ASTEC+ASTFIT (JCD, Christensen-Dalsgaard 2008) [**modelers: please correct/suggest additional references here, both for models and methods**]. Model inputs included the spectroscopic temperature and metallicity, individual frequencies, $\Delta\nu$, and the Gaia luminosity (Section 2.3). To investigate the effects of different input parameters, modelers were asked to provide solutions using both individual frequencies and only using $\Delta\nu$, with and without taking into account the luminosity constraints from Gaia.

The modeling efforts yielded overall consistent results, and most modeling codes were able to provide adequate fits to the observed oscillation frequencies (Figure 4). Independent analyses confirmed a bimodality in the modeling solutions splitting into lower-mass, older models ($\approx 1.15 M_\odot$, ≈ 6 Gyr) and higher-mass, younger models ($\approx 1.3 M_\odot$, ≈ 4 Gyr). Surface rotation would provide an independent mass diagnostic (e.g. van Saders & Pinsonneault 2013), but the current constraints on $v \sin i$ and the unknown stellar inclination are insufficient to decisively break this degeneracy. To account for the bimodality we adopted the solution of the modelling result with the mass closest to the median mass over all individual frequency results including the Gaia luminosity constraint, with uncertainties calculated by adding

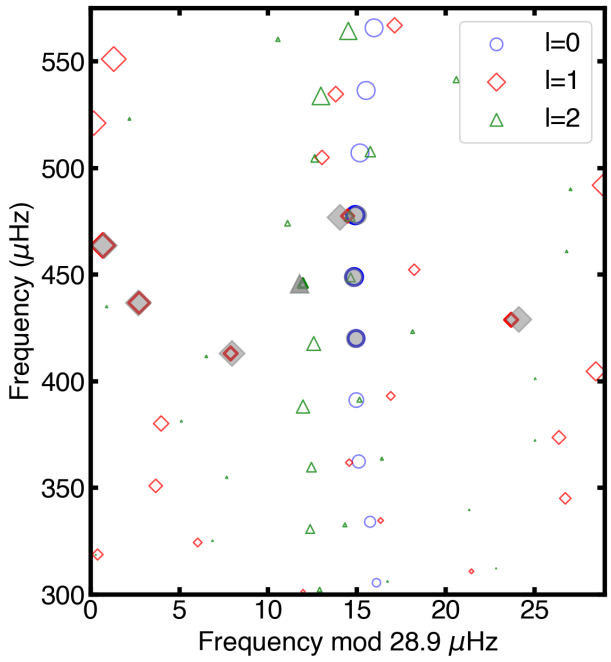

Figure 4. Échelle diagram showing observed oscillation frequencies (filled grey symbols) and a representative best-fitting model (open colored symbols) from the GARSTEC+BeSSP method (AS, Serenelli et al. 2013, 2017). Model symbol sizes are scaled by the inverse mode inertia (a proxy for mode amplitude). Thick model symbols correspond to modes that were matched to observations. Uncertainties on the observed frequencies are smaller or comparable to the symbol sizes.

the median uncertainty from all methods in quadrature to the standard deviation over all methods. The final estimates of stellar parameters are summarized in Table 2, constraining the radius, mass, density and age of TOI-197 to $\approx 2\,\%$, $\approx 7\,\%$, $\approx 2\,\%$ and $\approx 25\,\%$. We emphasize that our approach ensures that these uncertainties are robust against systematic errors by including realistic contributions from uncertainties due to input model physics.

4. PLANET CHARACTERIZATION

To fit the transits observed in the *TESS* data we used the PDC-MAP light curve provided by the TESS Science Processing and Operations Center (SPOC), which has been optimized to remove instrumental variability and preserve transits. To optimize computation time we discarded all data 2.5 days before and after each of the two observed transits. We have repeated the fit and data preparation procedure using the TASOC light curve and found consistent results.

Table 2. Host Star Parameters

Basic Properties	
Hipparcos ID	116158
TIC ID	441462736
V Magnitude	8.15
TESS Magnitude	7.30
SED & Gaia Parallax	
Parallax, π (mas)	10.5180 ± 0.0795
Luminosity, L ($L_\odot$)	5.15 ± 0.17
Spectroscopy	
Effective Temperature, $T_{\rm eff}$ (K)	5080 ± 90
Metallicity, [Fe/H] (dex)	-0.08 ± 0.08
Projected rotation speed, $v \sin i$ (km s^{-1})	2.8 ± 1.6
Asteroseismology	
Stellar Mass, $M_\star$ ($M_\odot$)	1.198 ± 0.081
Stellar Radius, $R_\star$ ($R_\odot$)	2.936 ± 0.061
Stellar Density, $\rho_\star$ (gcc)	0.0668 ± 0.0037
Surface gravity, $\log g$ (cgs)	3.581 ± 0.006
Age (Gyr)	5.04 ± 1.26

Table 3. High-precision Radial Velocities for TOI-197

Time (BJD)	RV (m/s)	$\sigma_{\rm RV}$ (m/s)	Instrument
2458426.334584	5.300	11.090	SONG
2458426.503655	7.570	10.960	SONG
2458427.575230	-4.490	3.000	FEROS
2458428.547576	17.840	18.430	SONG
2458428.581650	-8.790	3.000	FEROS
2458429.330382	0.220	8.290	SONG
2458430.319442	-9.880	9.290	SONG
2458430.623030	-19.690	3.000	FEROS
2458430.627110	-19.590	3.000	FEROS
2458430.631190	-23.790	3.000	FEROS
2458431.328588	-4.790	9.740	SONG
2458432.320066	-11.140	7.280	SONG
2458433.338667	-2.060	7.660	SONG
2458435.600800	6.010	5.400	CORALIE
2458435.610880	12.910	5.100	CORALIE
2458436.648500	10.610	4.300	CORALIE
2458436.683590	7.210	4.100	CORALIE
2458436.764789	16.437	0.900	HIRES
2458437.624110	14.510	3.500	CORALIE
...	...	...	...

Notes: Error bars do not include contributions from stellar jitter and measurements have not been corrected for zeropoint offsets.

A total of 79 radial velocity measurements from 4 different instruments (see Section 2.2 and Table 3) were used to constrain the mass of the planet. We performed a joint transit and radial velocity fit using Markov Chain Monte Carlo algorithm based on the exoplanet modeling code `ktransit` (Barclay 2018), as described in Chontos et al. (2018). We placed a strong Gaussian prior on the mean stellar density using the value derived from asteroseismology (Table 2) and weak priors on the linear and quadratic limb darkening coefficients, derived from the closest I-band grid points in Claret & Bloemen (2011) with a width of 0.6. We also adopted a prior for the radial velocity jitter from granulation and oscillations of $2.5 \pm 1.5\,{\rm m\,s^{-1}}$, following Yu et al. (2018), and fitted independent zeropoint offsets and stellar jitter values for each of the four instruments that provided radial velocities. Independent joint fits using EXOFASTv2 (Eastman et al. 2013) and **[exoplanet modelers: please provide references here]** yielded consistent results [tbc].

Figure 5 shows the best-fitting model and the summary statistics for all planet and model parameters are listed in Table 4. The system is well described by a planet in in a 14.3 day orbit which is near equal in size but $\approx$35% less massive than Saturn ($R_{\rm p} = 0.841 \pm 0.031\,R_{\rm J}$, $M_{\rm p} = 0.191 \pm 0.017\,M_{\rm J}$), with tentative evidence for a mild eccentricity ($e = 0.11 \pm 0.03$). The long transit duration ($\approx$0.5 days) is consistent with a non-grazing ($b \approx 0.7$) transit given the asteroseismic mean stellar density, providing further confirmation for a gas-giant planet orbiting an evolved star. The radial velocity data do not show evidence for a non-transiting companion. Continued monitoring past the $\approx$4 orbital periods covered here will further reveal details about the orbital architecture of this system, in particular the eccentricity of TOI-197.01.

5. DISCUSSION

TOI-197.01 joins an enigmatic but growing class of transiting planets orbiting stars which have significantly evolved off the main sequence. Figure 6 compares the position of TOI-197 within the expected population of solar-like oscillators to be detected with *TESS* (panel a) and within the known population of exoplanet host stars. Evolutionary states in Figure 6b have been assigned using solar-metallicity Parsec evolutionary tracks (Bressan et al. 2012) as described in Berger et al. (2018)[4] and demonstrate that TOI-197 sits right at the bound-

[4] see also https://github.com/danxhuber/evolstate

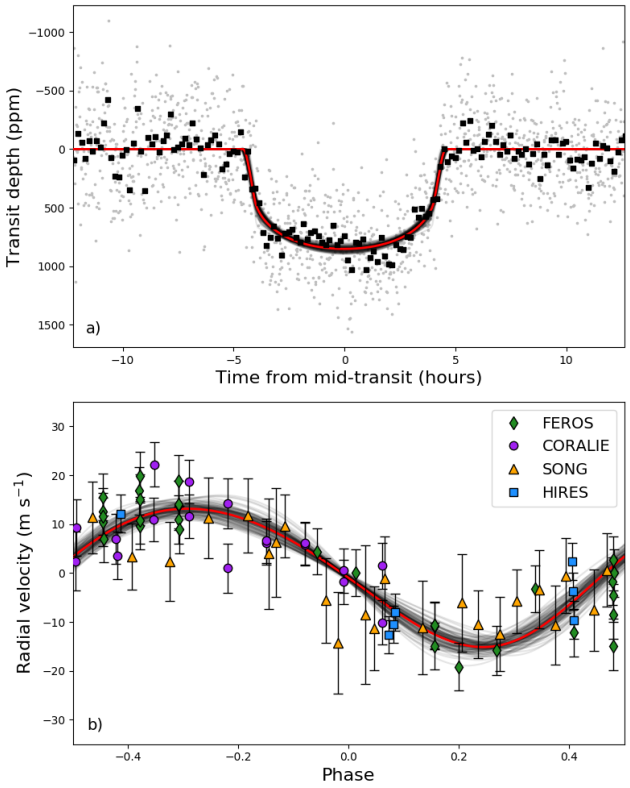

Figure 5. TESS light curve (panel a) and radial-velocity measurements (panel b) folded with best fitting orbital period. The red line shows the best-fitting model from the joint fit using stellar parameters, transit and radial-velocities. Grey lines show random draws from the joint MCMC model. Error bars in panel b include contributions from stellar jitter.

Table 4. Planet Parameters

Parameter	Best-fit	Median	84%	16%
Model Parameters				
$\gamma_{\rm HIRES}$	4.435	4.271	1.515	1.513
$\gamma_{\rm SONG}$	0.650	1.323	1.751	1.734
$\gamma_{\rm FEROS}$	-9.583	-8.912	1.009	1.010
$\gamma_{\rm CORALIE}$	3.932	3.618	1.229	1.224
$\sigma_{\rm HIRES}$	3.908	3.747	0.701	0.619
$\sigma_{\rm SONG}$	2.486	2.227	0.928	0.910
$\sigma_{\rm FEROS}$	3.622	3.708	0.654	0.627
$\sigma_{\rm CORALIE}$	2.621	2.703	0.827	0.844
z (ppm)	206.896	199.170	10.433	10.436
P (days)	14.27560	14.27628	0.00386	0.00383
T_0 (BKJD)	3524.0141	3524.0151	0.0026	0.0026
b	0.7378	0.7492	0.0433	0.0523
$R_p/R_\star$	0.02848	0.02883	0.00098	0.00080
$e\cos\omega$	-0.050	-0.056	0.071	0.071
$e\sin\omega$	-0.08256	-0.07011	0.02689	0.02889
K (m/s)	14.32118	14.14589	1.02603	1.03553
$\rho_\star$ (gcc)	0.066281	0.066770	0.003646	0.003702
Derived Properties				
e	0.097	0.107	0.043	0.034
a (AU)	0.12352	0.12233	0.00268	0.00281
$a/R_\star$	9.138	8.960	0.275	0.272
i (°)	85.712	85.509	0.394	0.410
ω	-121.26	-127.67	48.78	29.07
$R_{\rm p}(R_\oplus)$	9.041	9.247	0.369	0.324
$R_{\rm p}(R_{\rm J})$	0.8239	0.8427	0.0336	0.0295
$M_{\rm p}(M_\oplus)$	62.375	60.184	5.276	5.142
$M_{\rm p}(M_{\rm J})$	0.1962	0.1894	0.0166	0.0162
$\rho_{\rm p}$ (gcc)	0.465	0.419	0.063	0.059

ary between subgiants and red giants. TOI-197 is a typical target for which we expect to detect solar-like oscillations with *TESS*, predominantly due to the increased oscillation amplitude which are well known to scale with luminosity (Kjeldsen & Bedding 1995). On the contrary, TOI-197 is rare among exoplanet hosts: while radial velocity searches have uncovered a large number of planets orbiting red giants on long orbital periods (e.g. Wittenmyer et al. 2011), less than 15 transiting planets are known around evolved stars. TOI-197 is the sixth example of a transiting planet orbiting an evolved star with detected oscillations, following Kepler-91 (Barclay et al. 2013), Kepler-56 (Steffen et al. 2012; Huber et al. 2013b), Kepler-432 (Quinn et al. 2015), K2-97 (Grunblatt et al. 2016) and K2-132 (Grunblatt et al. 2017; Jones et al. 2018).

Transiting planets orbiting evolved stars are excellent systems to advance our understanding of the effects of stellar evolution on the structure and evolution of planets (see e.g. Veras 2016, for a review). For example, the evolution of the incident flux on the planet caused by the evolution of the host star has been proposed as a smoking gun to distinguish between proposed mechanisms to explain the inflation of radii of gas-giant planets beyond the limits expected from gravitational contraction and cooling (Hubbard et al. 2002; Lopez & Fortney 2013). Recent discoveries by the K2 Mission have indeed yielded evidence that planets orbiting low-luminosity RGB stars are consistent with being inflated by the evolution of the host star (Grunblatt et al. 2016, 2017), favoring scenarios in which the energy from the star is deposited into the deep planetary interior (Bodenheimer et al. 2001).

Based on its radius and orbital period TOI-197 would nominally be classified as a warm Saturn, sitting be-

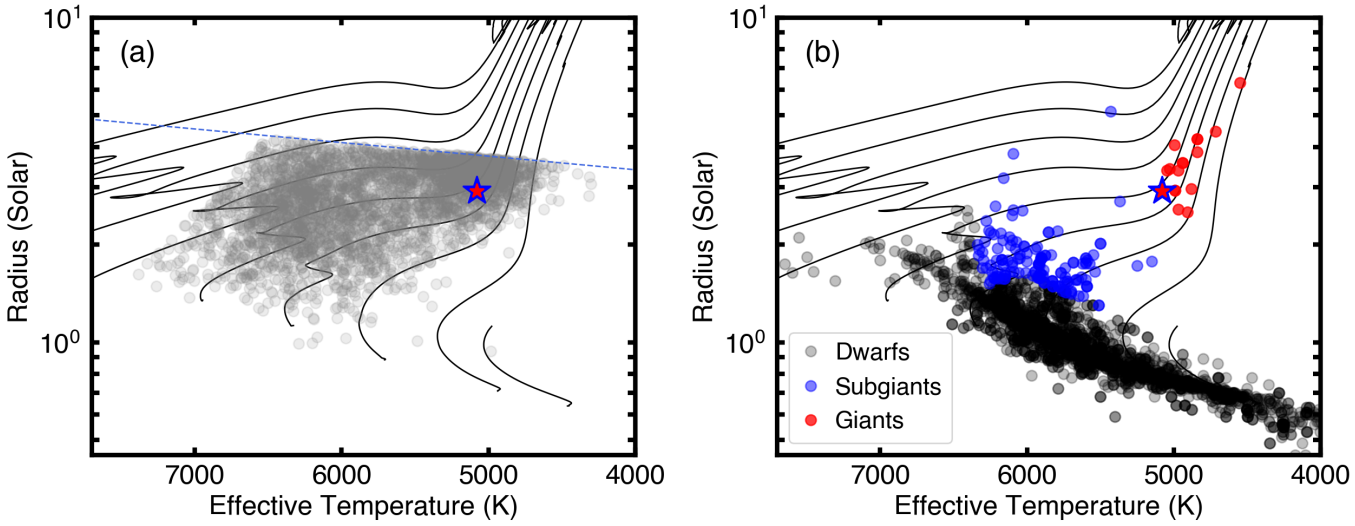

Figure 6. Stellar radius versus effective temperature for the expected yield of solar-like oscillators with *TESS* in Cycle 1 (panel a, Schofield et al. 2018) and for all stars with confirmed transiting planets (panel b). The blue dashed line in panel a marks the Nyquist limit for the 30-minute sampling of *TESS* full-frame images. Symbols in panel b are color-coded according to the rough evolutionary state of the host star using solar-metallicity Parsec evolutionary tracks. TOI-197 falls on the border between subgiants and red-giants, and is highlighted in both panels with red/blue star symbol. TOI-197 is a typical target for which we expect to detect solar-like oscillations with TESS, but occupies a rare parameter space for an exoplanet host.

tween the well-known population of hot Jupiters and the ubiquitous population of sub-Neptunes uncovered by Kepler (Figure 7a). Taking into account the evolutionary state of the host star, however, TOI-197 falls right at the beginning of the "inflation sequence" in the radius-incident flux diagram (Figure 7b), with planet radius strongly increasing with stellar incident flux (Miller & Fortney 2011). Since TOI-197.01 is currently clearly not inflated and low-mass planets are expected to be more susceptible to planet reinflation (Lopez & Fortney 2013), TOI-197 may thus be a progenitor of a class of re-inflated gas-giant planets orbiting RGB stars. If confirmed, the mild eccentricity TOI-197.01 would also be consistent with predictions of a population of planets around evolved stars for which orbital decay occurs faster than tidal circularization (Villaver et al. 2014; Grunblatt et al. 2018).

The precise characterization of planets orbiting evolved, oscillating stars also provide valuable insights into the diversity of compositions of planets. TOI-197.01 falls in the transition region between Neptune and sub-Saturn sized planets for which radii increase as $R_P \sim M_P^{0.6}$, and Jovian planets for which radius is nearly constant with mass (Weiss et al. 2013; Chen & Kipping 2017, Figure 8). Petigura et al. (2017b) found that the population of sub-Saturns ($\approx 4-8R_\oplus$) also displays a wide variety of densities, ranging from $\approx 6-60M_\oplus$ regardless of size. Furthermore, they found that planet mass correlates strongly with stellar metallicity, suggesting that metal-rich disks form more massive planet cores. TOI-197.01, which is larger than the population of sub-Saturns studied by Petigura et al. (2017b), does not follow this trend with a mass of $\approx 60M_\oplus$ and a slightly sub-solar metallicity host star ([Fe/H] ≈ -0.08 dex). This suggests that Saturn-sized planets may follow a relatively narrow range of densities, a possible signature of the transition in the interior structure (such as the increased importance of electron degeneracy pressure, Zapolsky & Salpeter 1969) leading to different mass-radius relations between sub-Saturns and Jupiters. We note that TOI-197.01 is one the most precisely characterized Saturn-sized planets to date, with a density uncertainty $\approx 15\%$. The uncertainty is dominated by the radial velocity semi-amplitude, and thus can be expected to further decrease with continued RV follow-up.

6. CONCLUSIONS

We have presented the discovery of TOI-197.01, the first transiting planet orbiting an oscillating host star identified by *TESS*. Our main conclusions are as follows:

- TOI-197 is an evolved subgiant with a clear presence of mixed modes. Combined spectroscopy and asteroseismic modeling revealed that the star sits at the base of the red giant branch, with $R_\star = 2.936 \pm 0.061 R_\odot$, $M_\star = 1.198 \pm 0.081 M_\odot$ and near-solar age (5.04 ± 1.26 Gyr). TOI-197 is a typical oscillating star expected to be detected

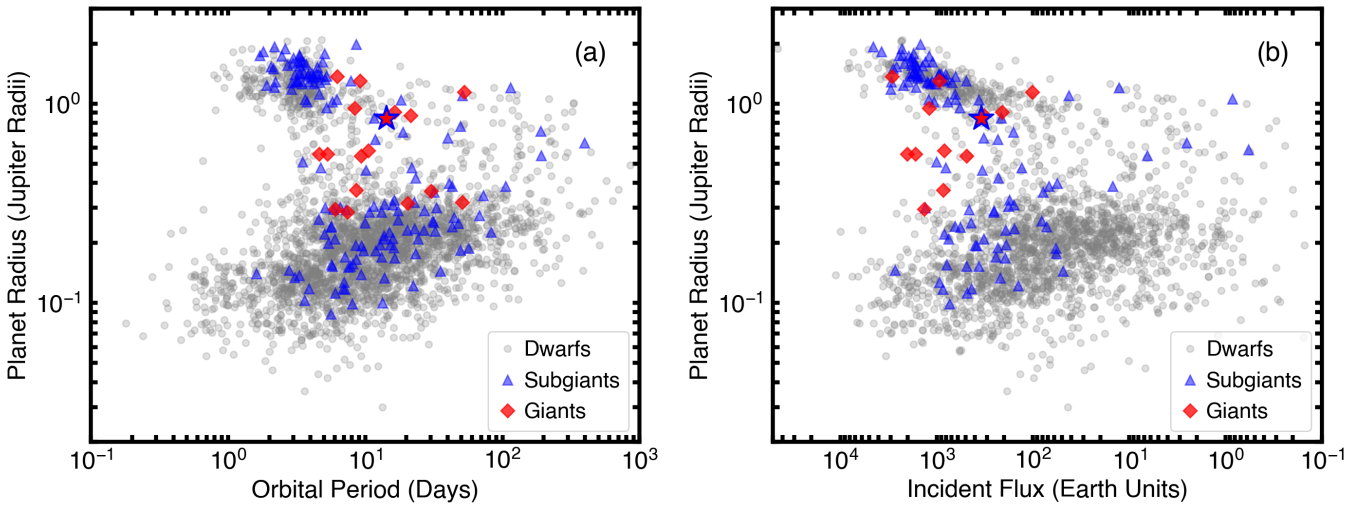

Figure 7. Planet radius versus orbital period (panel a) and incident flux (panel b) for confirmed exoplanets. Symbols are color-coded according to the evolutionary state of the host star (see Figure 6. TOI-197 b is highlighted in both panels with red/blue star symbol.

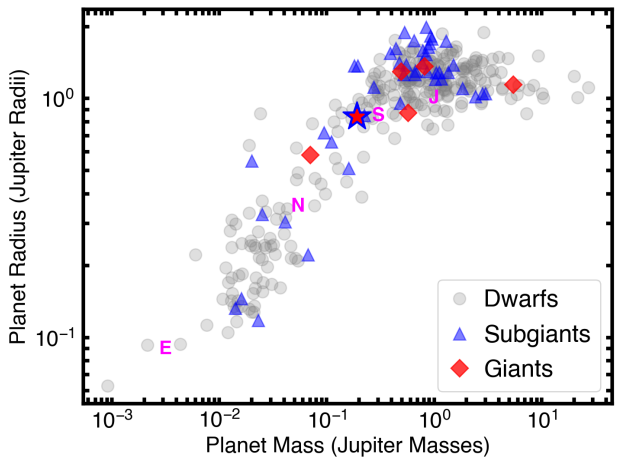

Figure 8. Mass-radius diagram for all confirmed planets with densities measured to better than 50%. Symbols are color-coded according to the evolutionary state of the host star (see Figure 6. TOI-197 b is highlighted in both panels with red/blue star symbol. Magenta letters show the position of solar system planets.

with *TESS*, and demonstrates the power of asteroseismology even with only 27 days of data.

- The oscillation amplitude of TOI-197 is consistent with ensemble measurements from Kepler. This confirms that the redder bandpass compared to Kepler only has a small effect on the oscillation amplitude, and validates the expected asteroseismic yield of thousands of detections of solar-like oscillators with TESS (Schofield et al. 2018).

- TOI-197.01 is a hot Saturn ($F = 344 \pm 27 F_\oplus$, $R_\mathrm{p} = 0.841 \pm 0.031\,R_\mathrm{J}$, $M_\mathrm{p} = 0.191 \pm 0.017\,M_\mathrm{J}$) and joins a small but growing population of planets orbiting evolved stars. Based on its incident flux, radius and mass, TOI-197 may be a precursor to the population of gas giants that undergo radius re-inflation due to the evolution of their host star.

- TOI-197.01 is one the most precisely characterized Saturn-sized planets to date, with a density measured to $\approx$15%. TOI-197.01 does not follow the trend of increasing planet mass with host star metallicity discovered in sub-Saturns, which has been linked to metal-rich disks preferentially forming more massive planet cores (Petigura et al. 2017b). The moderate density ($\rho_\mathrm{p} = 0.424 \pm 0.060\,\mathrm{g\,cm^{-3}}$) suggests that Saturn-sized planets may follow a relatively narrow range of densities, a possible signature of the transition in the interior structure leading to different mass-radius relations for sub-Saturns and Jupiters.

TOI-197 provides a first glimpse at the strong potential of *TESS* to characterize exoplanets using asteroseismology. Continued radial velocity follow-up of TOI-197 will significantly improve the constraint on the mean stellar density and eccentricity of the planet. Ensemble studies of such precisely characterized planets orbiting oscillating subgiants can be expected to yield significant new insights on the effects of stellar evolution on exoplanets, complementing current intensive efforts to characterize planets orbiting cool dwarfs.

The authors wish to recognize and acknowledge the very significant cultural role and reverence that the summit of Maunakea has always had within the indigenous Hawai'ian community. We are most fortunate to have the opportunity to conduct observations from this mountain. D.H. acknowledges support by the National Aeronautics and Space Administration through the TESS Guest Investigator Program (80NSSC18K1585) and by the National Science Foundation (AST-1717000). A.C. acknowledges support by the National Science Foundation under the Graduate Research Fellowship Program.

Funding for the TESS mission is provided by NASA's Science Mission directorate. We acknowledge the use of public TESS Alert data from pipelines at the TESS Science Office and at the TESS Science Processing Operations Center. This research has made use of the Exoplanet Follow-up Observation Program website, which is operated by the California Institute of Technology, under contract with the National Aeronautics and Space Administration under the Exoplanet Exploration Program. This paper includes data collected by the TESS mission, which are publicly available from the Mikulski Archive for Space Telescopes (MAST).

REFERENCES

Appourchaux, T., Chaplin, W. J., García, R. A., et al. 2012, A&A, 543, A54, doi: 10.1051/0004-6361/201218948

Ballard, S., Chaplin, W. J., Charbonneau, D., et al. 2014, ApJ, 790, 12, doi: 10.1088/0004-637X/790/1/12

Ballot, J., Gizon, L., Samadi, R., et al. 2011, A&A, 530, A97, doi: 10.1051/0004-6361/201116547

Barclay, T. 2018, ktransit: Exoplanet transit modeling tool in python, Astrophysics Source Code Library. http://ascl.net/1807.028

Barclay, T., Rowe, J. F., Lissauer, J. J., et al. 2013, Nature, 494, 452, doi: 10.1038/nature11914

Bastien, F. A., Stassun, K. G., Basri, G., & Pepper, J. 2013, Nature, 500, 427, doi: 10.1038/nature12419

Basu, S., & Chaplin, W. J. 2017, Asteroseismic Data Analysis: Foundations and Techniques

Bazot, M., Vauclair, S., Bouchy, F., & Santos, N. C. 2005, A&A, 440, 615, doi: 10.1051/0004-6361:20052698

Bedding, T. R., Kjeldsen, H., Arentoft, T., et al. 2007, ApJ, 663, 1315, doi: 10.1086/518593

Bell, K. J., Hekker, S., & Kuszlewicz, J. S. 2019, MNRAS, 482, 616, doi: 10.1093/mnras/sty2731

Benomar, O., Masuda, K., Shibahashi, H., & Suto, Y. 2014, PASJ, doi: 10.1093/pasj/psu069

Berger, T. A., Huber, D., Gaidos, E., & van Saders, J. L. 2018, ArXiv e-prints. https://arxiv.org/abs/1805.00231

Bodenheimer, P., Lin, D. N. C., & Mardling, R. A. 2001, ApJ, 548, 466, doi: 10.1086/318667

Bouchy, F., Bazot, M., Santos, N. C., Vauclair, S., & Sosnowska, D. 2005, A&A, 440, 609, doi: 10.1051/0004-6361:20052697

Bovy, J., Rix, H.-W., Green, G. M., Schlafly, E. F., & Finkbeiner, D. P. 2016, ApJ, 818, 130, doi: 10.3847/0004-637X/818/2/130

Bressan, A., Marigo, P., Girardi, L., et al. 2012, MNRAS, 427, 127, doi: 10.1111/j.1365-2966.2012.21948.x

Campante, T. L. 2018, Asteroseismology and Exoplanets: Listening to the Stars and Searching for New Worlds, 49, 55, doi: 10.1007/978-3-319-59315-9_3

Campante, T. L., Schofield, M., Kuszlewicz, J. S., et al. 2016, ApJ, 830, 138, doi: 10.3847/0004-637X/830/2/138

Chaplin, W. J., & Miglio, A. 2013, ARA&A, 51, 353, doi: 10.1146/annurev-astro-082812-140938

Chaplin, W. J., Basu, S., Huber, D., et al. 2014, ApJS, 210, 1, doi: 10.1088/0067-0049/210/1/1

Chen, J., & Kipping, D. 2017, ApJ, 834, 17, doi: 10.3847/1538-4357/834/1/17

Choi, J., Dotter, A., Conroy, C., et al. 2016, ApJ, 823, 102, doi: 10.3847/0004-637X/823/2/102

Chontos, A., Burt, J., Vanderburg, A., et al. 2018, ApJ, submitted. https://arxiv.org/abs/1809.05967

Christensen-Dalsgaard, J. 2008, Ap&SS, 316, 13, doi: 10.1007/s10509-007-9675-5

Claret, A., & Bloemen, S. 2011, A&A, 529, A75, doi: 10.1051/0004-6361/201116451

Corsaro, E., & De Ridder, J. 2014, A&A, 571, A71, doi: 10.1051/0004-6361/201424181

Corsaro, E., Fröhlich, H.-E., Bonanno, A., et al. 2013, MNRAS, 430, 2313, doi: 10.1093/mnras/stt059

Creevey, O. L., Metcalfe, T. S., Schultheis, M., et al. 2017, A&A, 601, A67, doi: 10.1051/0004-6361/201629496

Davies, G. R., & Miglio, A. 2016, Astronomische Nachrichten, 337, 774, doi: 10.1002/asna.201612371

Demarque, P., Guenther, D. B., Li, L. H., Mazumdar, A., & Straka, C. W. 2008, Ap&SS, 316, 31, doi: 10.1007/s10509-007-9698-y

Eastman, J., Gaudi, B. S., & Agol, E. 2013, PASP, 125, 83, doi: 10.1086/669497

Evans, D. W., Riello, M., De Angeli, F., et al. 2018, A&A, 616, A4, doi: 10.1051/0004-6361/201832756

Fulton, B. J., Petigura, E. A., Howard, A. W., et al. 2017, AJ, 154, 109, doi: 10.3847/1538-3881/aa80eb

Fürész, G. 2008, PhD thesis, University of Szeged, Szeged, Hungary
Gilliland, R. L., McCullough, P. R., Nelan, E. P., et al. 2011, ApJ, 726, 2, doi: 10.1088/0004-637X/726/1/2
Grunblatt, S. K., Huber, D., Gaidos, E. J., et al. 2016, AJ, 152, 185, doi: 10.3847/0004-6256/152/6/185
Grunblatt, S. K., Huber, D., Gaidos, E., et al. 2017, AJ, 154, 254, doi: 10.3847/1538-3881/aa932d
—. 2018, ApJL, 861, L5, doi: 10.3847/2041-8213/aacc67
Grundahl, F., Fredslund Andersen, M., Christensen-Dalsgaard, J., et al. 2017, ApJ, 836, 142, doi: 10.3847/1538-4357/836/1/142
Handberg, R., & Lund, M. N. 2014, MNRAS, 445, 2698, doi: 10.1093/mnras/stu1823
Hekker, S., Elsworth, Y., De Ridder, J., et al. 2011, A&A, 525, A131, doi: 10.1051/0004-6361/201015185
Høg, E., Fabricius, C., Makarov, V. V., et al. 2000, A&A, 355, L27
Hubbard, W. B., Burrows, A., & Lunine, J. I. 2002, ARA&A, 40, 103, doi: 10.1146/annurev.astro.40.060401.093917
Huber, D., Stello, D., Bedding, T. R., et al. 2009, Communications in Asteroseismology, 160, 74. https://arxiv.org/abs/0910.2764
Huber, D., Bedding, T. R., Arentoft, T., et al. 2011, ApJ, 731, 94, doi: 10.1088/0004-637X/731/2/94
Huber, D., Chaplin, W. J., Christensen-Dalsgaard, J., et al. 2013a, ApJ, 767, 127, doi: 10.1088/0004-637X/767/2/127
Huber, D., Carter, J. A., Barbieri, M., et al. 2013b, Science, 342, 331. https://arxiv.org/abs/1310.4503
Huber, D., Bryson, S. T., Haas, M. R., et al. 2017, ApJ, 224, 2, doi: 10.3847/0067-0049/224/1/2
Johnson, J. A., Petigura, E. A., Fulton, B. J., et al. 2017, AJ, 154, 108, doi: 10.3847/1538-3881/aa80e7
Jones, M. I., Brahm, R., Espinoza, N., et al. 2018, A&A, 613, A76, doi: 10.1051/0004-6361/201731478
Kallinger, T., Beck, P. G., Stello, D., & Garcia, R. A. 2018, A&A, 616, A104, doi: 10.1051/0004-6361/201832831
Kaufer, A., Stahl, O., Tubbesing, S., et al. 1999, The Messenger, 95, 8
Kjeldsen, H., & Bedding, T. R. 1995, A&A, 293, 87
Kjeldsen, H., Bedding, T. R., Butler, R. P., et al. 2005, ApJ, 635, 1281, doi: 10.1086/497530
Kjeldsen, H., Bedding, T. R., Arentoft, T., et al. 2008, ApJ, 682, 1370, doi: 10.1086/589142
Lebreton, Y., & Goupil, M. J. 2014, A&A, 569, A21, doi: 10.1051/0004-6361/201423797
Lopez, E. D., & Fortney, J. J. 2013, ApJ, 776, 2, doi: 10.1088/0004-637X/776/1/2
Lund, M. N., Handberg, R., Davies, G. R., Chaplin, W. J., & Jones, C. D. 2015, ApJ, 806, 30, doi: 10.1088/0004-637X/806/1/30
Lund, M. N., Handberg, R., Kjeldsen, H., Chaplin, W. J., & Christensen-Dalsgaard, J. 2017, in European Physical Journal Web of Conferences, Vol. 160, European Physical Journal Web of Conferences, 01005
Lund, M. N., Chaplin, W. J., Casagrande, L., et al. 2016, PASP, 128, 124204, doi: 10.1088/1538-3873/128/970/124204
Lundkvist, M. S., Kjeldsen, H., Albrecht, S., et al. 2016, Nature Communications, 7, 11201, doi: 10.1038/ncomms11201
Mathur, S., García, R. A., Régulo, C., et al. 2010, A&A, 511, A46, doi: 10.1051/0004-6361/200913266
Miller, N., & Fortney, J. J. 2011, ApJL, 736, L29, doi: 10.1088/2041-8205/736/2/L29
Morel, P., & Lebreton, Y. 2008, Ap&SS, 316, 61, doi: 10.1007/s10509-007-9663-9
Mosser, B., Elsworth, Y., Hekker, S., et al. 2012a, A&A, 537, A30, doi: 10.1051/0004-6361/201117352
Mosser, B., Goupil, M. J., Belkacem, K., et al. 2012b, A&A, 548, A10, doi: 10.1051/0004-6361/201220106
Paxton, B., Bildsten, L., Dotter, A., et al. 2011, ApJS, 192, 3, doi: 10.1088/0067-0049/192/1/3
Paxton, B., Cantiello, M., Arras, P., et al. 2013, ApJS, 208, 4, doi: 10.1088/0067-0049/208/1/4
Paxton, B., Marchant, P., Schwab, J., et al. 2015, ApJS, 220, 15, doi: 10.1088/0067-0049/220/1/15
Petigura, E. A., Howard, A. W., Marcy, G. W., et al. 2017a, AJ, 154, 107, doi: 10.3847/1538-3881/aa80de
Petigura, E. A., Sinukoff, E., Lopez, E. D., et al. 2017b, AJ, 153, 142, doi: 10.3847/1538-3881/aa5ea5
Quinn, S. N., White, T. R., Latham, D. W., et al. 2015, ApJ, 803, 49, doi: 10.1088/0004-637X/803/2/49
Ricker, G. R., Winn, J. N., Vanderspek, R., et al. 2014, in Society of Photo-Optical Instrumentation Engineers (SPIE) Conference Series, Vol. 9143, , 20
Schlegel, D. J., Finkbeiner, D. P., & Davis, M. 1998, ApJ, 500, 525, doi: 10.1086/305772
Schofield, M., Burt, J., Vanderburg, A., et al. 2018, ArXiv e-prints. https://arxiv.org/abs/1809.05967
Scuflaire, R., Montalbán, J., Théado, S., et al. 2008, Ap&SS, 316, 149, doi: 10.1007/s10509-007-9577-6
Serenelli, A., Johnson, J., Huber, D., et al. 2017, ApJS, 233, 23, doi: 10.3847/1538-4365/aa97df
Serenelli, A. M., Bergemann, M., Ruchti, G., & Casagrande, L. 2013, MNRAS, 429, 3645, doi: 10.1093/mnras/sts648
Silva Aguirre, V., Davies, G. R., Basu, S., et al. 2015, MNRAS, 452, 2127, doi: 10.1093/mnras/stv1388

Skrutskie, M. F., Cutri, R. M., Stiening, R., et al. 2006, AJ, 131, 1163, doi: 10.1086/498708

Sliski, D. H., & Kipping, D. M. 2014, ApJ, 788, 148, doi: 10.1088/0004-637X/788/2/148

Stassun, K. G., & Torres, G. 2016, AJ, 152, 180, doi: 10.3847/0004-6256/152/6/180

—. 2018, ApJ, 862, 61, doi: 10.3847/1538-4357/aacafc

Steffen, J. H., Ragozzine, D., Fabrycky, D. C., et al. 2012, Proceedings of the National Academy of Science, 109, 7982, doi: 10.1073/pnas.1120970109

Stello, D., Zinn, J., Elsworth, Y., et al. 2017, ApJ, 835, 83, doi: 10.3847/1538-4357/835/1/83

Tayar, J., & Pinsonneault, M. H. 2018, ArXiv e-prints. https://arxiv.org/abs/1806.10649

Torres, G., Fischer, D. A., Sozzetti, A., et al. 2012, ApJ, 757, 161, doi: 10.1088/0004-637X/757/2/161

Townsend, R. H. D., & Teitler, S. A. 2013, MNRAS, 435, 3406, doi: 10.1093/mnras/stt1533

Van Eylen, V., & Albrecht, S. 2015, ApJ, 808, 126, doi: 10.1088/0004-637X/808/2/126

Van Eylen, V., Albrecht, S., Huang, X., et al. 2018, ArXiv e-prints. https://arxiv.org/abs/1807.00549

van Saders, J. L., Ceillier, T., Metcalfe, T. S., et al. 2016, Nature, 529, 181, doi: 10.1038/nature16168

van Saders, J. L., & Pinsonneault, M. H. 2013, ApJ, 776, 67, doi: 10.1088/0004-637X/776/2/67

Veras, D. 2016, Royal Society Open Science, 3, 150571, doi: 10.1098/rsos.150571

Verner, G. A., Elsworth, Y., Chaplin, W. J., et al. 2011, MNRAS, 415, 3539, doi: 10.1111/j.1365-2966.2011.18968.x

Villaver, E., Livio, M., Mustill, A. J., & Siess, L. 2014, ApJ, 794, 3, doi: 10.1088/0004-637X/794/1/3

Vogt, S. S., Allen, S. L., Bigelow, B. C., et al. 1994, in Society of Photo-Optical Instrumentation Engineers (SPIE) Conference Series, Vol. 2198, Society of Photo-Optical Instrumentation Engineers (SPIE) Conference Series, ed. D. L. Crawford & E. R. Craine, 362

Weiss, L. M., Marcy, G. W., Rowe, J. F., et al. 2013, ApJ, 768, 14, doi: 10.1088/0004-637X/768/1/14

White, T. R., Bedding, T. R., Stello, D., et al. 2011, ApJ, 743, 161, doi: 10.1088/0004-637X/743/2/161

Wittenmyer, R. A., Endl, M., Wang, L., et al. 2011, ApJ, 743, 184, doi: 10.1088/0004-637X/743/2/184

Wizinowich, P., Acton, D. S., Shelton, C., et al. 2000, PASP, 112, 315, doi: 10.1086/316543

Wright, E. L., Eisenhardt, P. R. M., Mainzer, A. K., et al. 2010, AJ, 140, 1868, doi: 10.1088/0004-6256/140/6/1868

Yu, J., Huber, D., Bedding, T. R., & Stello, D. 2018, MNRAS, 480, L48, doi: 10.1093/mnrasl/sly123

Zapolsky, H. S., & Salpeter, E. E. 1969, ApJ, 158, 809, doi: 10.1086/150240